PHYSICAL REVIEW A VOLUME 35, NUMBER 10 MAY 15, 1987

# Dynamics of laser-irradiated planar targets measured by x-ray spectroscopy

R. L. Kauffman, R. W. Lee, and K. Estabrook
*Lawrence Livermore National Laboratory, University of California, P.O. Box 5508, Livermore, California 94550*
(Received 14 January 1987)

The dynamics of planar plastic targets seeded with small amounts of sulfur as a diagnostic tracer is studied spectroscopically. The time-dependent x-ray emission of the hydrogenic and heliumlike sulfur is used to provide a measure of the plasma parameters. The experiment, which is designed to provide optically thin x-ray lines with small transverse gradients, is analyzed by the coupling of a kinetics model to a hydrodynamics simulation. The results of the analysis show that the time histories of the x-ray line intensities can be used as a plasma diagnostic to constrain the modeling. Intensity ratios between ionization stages cannot be accurately modeled even including time-dependent ionization effects. This disagreement appears to be due to detailed assumptions concerning electron distributions and transport.

## I. INTRODUCTION

The coupling of high-powered lasers to dense matter can produce the highest-density and -temperature laboratory plasmas. Several applications of these high—energy-density plasmas have been suggested. They can be used to create inertially confined fusion by using the high-powered lasers to compress and heat small masses of deuterium and tritium fuel.[1] All facets of laser-plasma interactions, from energy deposition to plasma instabilities, are important in converting laser energy to useful fuel compression. Laser-produced plasmas can be bright x-ray sources which have applications in x-ray radiography and backlighting.[2] In addition, recent advances in the production of short wavelength lasers use laser-produced plasmas as the amplifying medium.[3] Detailed knowledge of the laser-plasma coupling mechanisms are required for optimizing these sources.

Fundamental to understanding laser-plasma interactions is detailed characterization of the plasma. Characterization of the plasma would ideally include spatially and temporally resolved information for both the plasma temperature and electron densities, as well as the ion-stage populations. However, obtaining all of this information is problematic for a number of reasons. First, laser-produced plasmas are rapidly formed by coupling laser energy to the target with thermal and radiative transport distributing the energy into the matter. These processes are not well understood on a microscopic scale. Second, the kinetics of a hot dense plasma are not simple. Gradients axially and laterally to the laser incident on the plasma preclude simple characterization of the plasma with a single temperature and density. In addition, the plasma reacts hydrodynamically on time scales different from the time scales for establishing steady state in the ionization kinetics. Thus ions may not sample one temperature and density but sample a variety of plasma conditions. Finally, the time and distance scales for substantial changes to occur in the emitting ion population can be smaller than the experimental temporal and spatial resolution currently possible. This leads to a loss of information and loss of uniqueness in the comparison between theory and experiments.

X-ray spectroscopy has been a successful method of understanding the high-energy laser-target interaction and of diagnosing the plasma. In particular, the applications of x-ray line spectroscopy, which use the intensity of bound-bound transitions to infer plasma parameters, is quite wide spread.[4,8] Plasma temperatures can be derived using the intensities of lines from different charge states, which reflect the ionization balance of the plasma. On the other hand, line intensities from transitions having decay rates comparable to electron collisional rates can give a measure of the electron density of the plasma. In this way, the x-ray line spectroscopy lends itself to simple analysis of the plasma. Another advantage is that the method can probe microscopic plasma volumes with measurements of localized areas. Also, the method requires no external probe to disturb the plasma. X-ray spectroscopy can access high-density regions which are difficult for external probes to penetrate. By extending the measurements to low densities, the technique can complement other methods, such as optical diagnostics, to provide a complete characterization of the plasma.

Although these advantages of x-ray spectroscopy are possible in ideal experiments, the fact remains that in practice many are compromised. The difficulties of observing and interpreting the x-ray emission spectra from previous experiments arise from a variety of sources. First, many of the observations are time averaged which causes a loss of information because of the rapidly changing state of ionization and other transient effects. Next, the limitation on spatial resolution causes a decrease in information due to the averaging over the longitudinal and transverse gradients present in the system. Finally, optical-depth effects or, more precisely, radiative-transfer effects can cause difficulty in interpreting the line intensities.

To mitigate these limitations, advances have been made during the last few years. Spot spectroscopy, where a seed element is placed in a limited area of the target to probe the plasma, has improved spatial information.[5] The use

 

of x-ray streak cameras and framing cameras has provided temporal resolution, allowing the complicated transient behavior of these laser-produced plasmas to be unfolded.[4,6]

In the current work we address a number of the outstanding difficulties with the x-ray line spectroscopy by combining several of the techniques for the first time. Firstly, the x-ray spectra are time resolved using an x-ray streak camera in order to study the transient in line production. Second, the targets are prepared with a low-density dopant, which keeps the optical depth of the lines low, thereby obviating radiative-transfer effects. Third, a spot of the seeded material is introduced to reduce the gradients transverse of the laser axis. This experimental design allows us to analyze data with only axial gradients that are perpendicular to the target surface. These axial gradients are included in the analysis by simulations. These techniques have been applied to analysis of dynamics of thin foil targets, i.e., targets that burn through becoming underdense to the laser light before the laser pulse is over. The foils provide plasma profiles that can be characterized by other methods allowing correlation of the spectroscopy with other diagnostic methods. Examples of these methods are optical spectroscopy of the $\frac{3}{2}\omega_0$,[9] Raman signal,[10] foil burn-through times,[11] and laser interferometry.[12] Such techniques constrain the simulations which establish the range of temperature and density profiles that are physically possible.

## II. EXPERIMENTAL SETUP

The experiments were performed at the Novette laser facility, a two-beam Nd-glass laser system with a final beam aperture of 74-cm diameter, which can produce up to 9 kJ of 1.05-$\mu$m light per beam in a 1-ns pulse.[13] The light is frequency converted before entering the target chamber to 0.53-$\mu$m wavelength using a potassium dihydrogen phosphate (KDP) crystal array. Beam energies varied up to 3 kJ in a 1-ns Guassian pulse shape which were focused to spot sizes from 300- to 600-$\mu$m diameter using an $f/4$ lens onto thin $CH_x$ foils. Average incident laser intensities on target varied from $5\times10^{14}$ to $2\times10^{15}$ W/cm$^2$. Beam structure deduced from x-ray microscope pictures may vary the local intensity at points inside the focal region by a factor of 2 from the average intensity. Both beam energies and time histories were measured by monitoring a reflection from one surface of the focusing lens after the conversion process. Energies of these reflections were calibrated independently on separate shots.

The $CH_x$ foil targets varied in thickness from 1.0 to 2.1 $\mu$m. The thicknesses and beam intensities were chosen to produce long scalelength, underdense plasmas around the peak of the laser pulse. A small concentration of sulfur was added uniformly to the $CH_x$ during deposition, which was used as the x-ray line spectroscopic diagnostic. Concentrations of sulfur were kept below 4% atomic in order not to change the dynamics of the plasma. In addition, these low concentrations reduced effects due to optical trapping in the experiments by keeping the optical depths of the measured x-ray lines below one. For some targets only the center 300 $\mu$m of the foil was doped with sulfur. This was accomplished by masking while depositing the doped and undoped regions. The thicknesses were matched in the two regions to better than 1000 Å except for a small interface between the two regions. The area of the interface is small compared to structure in the laser and scalelengths of the plasma and should not affect the results.

In Fig. 1 the experiment geometry is shown. The spectrometer viewed normal to the target and the laser was focused to an area larger than 4% sulfur-seeded spot. Figure 1 also shows the reflected and transmitted 0.53-$\mu$m laser light. This, therefore, illustrates the burnthrough of the laser during the pulse.

The primary diagnostic was a concave elliptical crystal, used as the light-collecting, wavelength-dispersing element, coupled to an x-ray streak camera.[14] The crystal was potassium acid phthalate (KAP) ($2d=26.632$ Å) and it was placed 1 m away from the camera. The cathode of the streak camera was located behind the ellipse focus. An example of the data is shown in Fig. 2 (a). The data were taken at a principal Bragg angle of 10.1°. The dispersion of the data is 74 eV/mm at the slit giving a resolution of 7 eV. The resolving power of the instrument is estimated to be $\sim200$. The $n=2$ to $n=1$ ($\alpha$) and $n=3$ to $n=1$ ($\beta$) features from the He-like and Lyman series are observed. The resolution is not sufficient to resolve the He-like intercombination line ($^3P_1$) from the resonance line ($^1P_1$).

The film data, as shown in Fig. 2(a), are analyzed by digitizing the film using a Perkin Elmer microdensitometer system producing a two-dimensional digital image of the film. Time histories of the data are extracted from the digitized images correcting for the nonlinear film response using calibrated light exposures placed on each piece of film data. As an example, the time histories for the heliumlike and resonance and Lyman $\alpha$ lines are shown in Fig. 2(b). The time resolution is $\sim50$ ps. Both time histories are approximately 350 ps at full width half max-

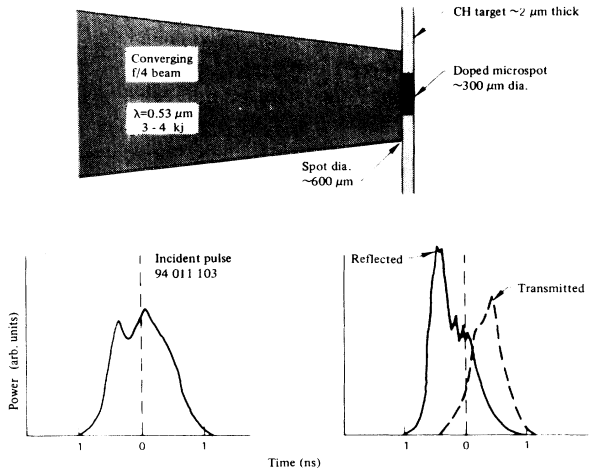


FIG. 1. The experimental geometry. Also shown are the reflected and transmitted laser light as a function of time, with the peak of the pulse noted by zero on the time axis.

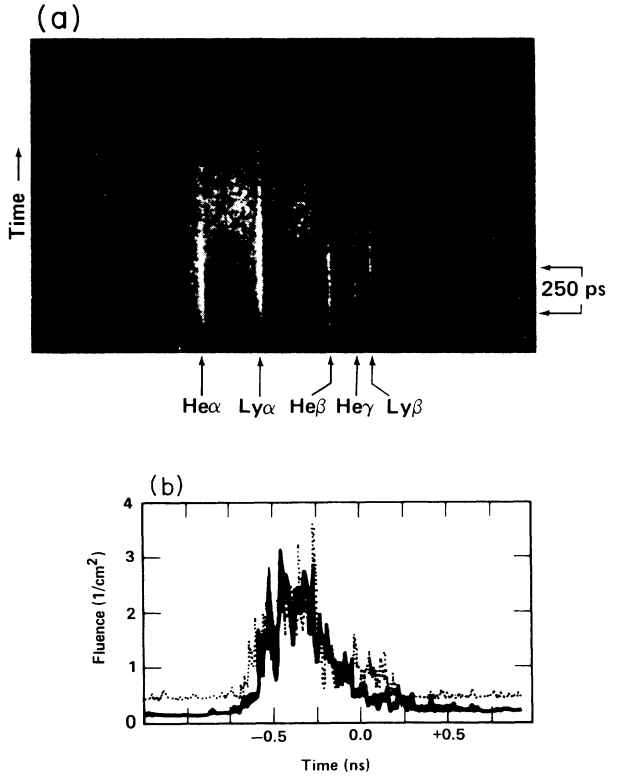


FIG. 2. Experimental results from the x-ray crystal streak camera. The raw data are shown in (a). Time is in the vertical direction and the dispersed x-ray spectrum in the horizontal direction. The heliumlike and hydrogenic sulfur lines are indicated. Time histories are shown in (b) of the S XV resonance ($R$) (bold solid curve) and S XVI Lyman-$\alpha$ (Ly-$\alpha$) (dashed curve) emission.

imum, which is considerably shorter than the 900-ps laser pulse. The time histories of both lines have a similar structure during the rising part of the pulse. On the trailing edge, however, the heliumlike resonance line intensity decreases more rapidly. This is presumably when the foil burns through, becoming underdense to the 0.53-$\mu$m laser light. There is continuum emission at late time around the heliumlike resonance line, which has been subtracted from the data. This allows only an upper limit to be set for several data points after burnthrough has occurred.

## III. HYDRODYNAMIC SIMULATIONS

To compare the experimental and theoretically calculated emission spectra, we use hydrodynamics simulation to model the plasma density and temperature profiles. The simulations predict the plasma gradients, in particular, those in the direction parallel to the laser beam which are not resolved in the observations. Further, the hydrodynamics simulation is used to test the validity of the assumptions concerning transverse gradients.

We used LASNEX, a two-dimensional, hydrodynamics simulation code, which treats energy transport using the flux-limited diffusion approximation. All simulations were done with a flux-limit multiplier of 0.03 of the classical limit in two dimensions, and with radiation transport treated using non—local-thermodynamic-equilibrium (non-LTE) opacities.[15] Zone sizes were chosen in order to resolve the ablation region at the front, as well as the burnthrough region at the back of the foil. Tests of the simulation parameters were performed by varying the modeling parameters and comparing with the experimental observables. The simulations indicated that the introduction of the sulfer in a concentration of 4% by atomic number produced a negligible perturbation of the foil hydrodynamics. Further, it was found that the non-LTE option, two dimensions, and the flux limit were essential to provide meaningful simulations.

Figures 3(a), 3(b), and 3(c) show results of the hydrodynamic simulations for the case of a 1-ns pulse of 0.53-$\mu$m light with an intensity of $1.3\times10^{15}$ W/cm$^2$ incident on the 2.1-$\mu$m-thick foil focused to a spot size of 600 $\mu$m. The three parts of Fig. 3 show the evolution of the foil in two dimensions, with the abscissa in the laser propagation direction and both axes measured in microns. The area which contains sulfur is noted by cross hatching. Further, temperature and density contours of interest are shown in each case for reference. The two-dimensional evolution is evident as the foil goes from overdense where peak densities are greater than $4\times10^{21}$ $e^-$/cm$^3$, at -0.6 ns (before the peak of the pulse which is at 0.0 ns), through -0.4 ns, to underdense where densities are less than $4\times10^{21}$ $e^-$/cm$^3$, at $+0.6$ ns.

The calculations corroborate that the foils do burn through before the peak of the pulse. Further, the transverse gradients in the spot are small, while the longitudinal gradients are large. Finally, the gradients are substantial outside the spot of sulfur in the transverse direction. This latter point will be shown to be important when analyzing targets which have 4% sulfur distributed uniformly over the whole target.

The detailed spectroscopy predictions are done using a kinetics model that treats the $K$-shell ionization stages in detail. We include ionization states up to lithiumlike states with a ground-state configuration only. The lithiumlike, heliumlike, and hydrogenic ion stages have both ground states, excited and doubly excited states; a fuller discussion of the kinetic code previously has been given by Lee *et al.*[16] The code assumes that the temperature provided by the hydrodynamic simulation is indicative of a Maxwellian velocity distribution. Further, we do not include the effects of radiative transport on the level populations since the optical depths in all the lines of interest are less than one.

We use the hydrodynamic time histories to drive the kinetics of the sulfur atoms. The consistency of this post-processing of detailed kinetics, using the time histories generated by a code employing an average atom non-LTE model, is checked by comparing the hydrodynamic electron density and mean ionization state to those calculated by the kinetics model. These are found to be within a few percent of each other for all cases in the present studies.

The timesteps for the kinetics equations are dictated by the kinetic rates, not the hydrodynamics, thereby ensuring numerical accuracy for the level populations. The final

results of importance are the heliumlike and hydrogenic resonance line emissions, which are found by integration over all the zones that contain sulfur. Thus, in the case of a sulfur spot, only the central zones are summed while all zones are included for targets with sulfur uniformly distributed over the whole.

## IV. COMPARISON OF THE CALCULATIONS WITH EXPERIMENTS

The calculations are compared to the experimental results by comparing time histories of the heliumlike S XV and hydrogenic S XVI resonance lines. The timing, and intensity normalizations, for comparison are done consistently using the following method. The S XV and S XVI emission for either calculation or experiment are fixed in time and intensity. We thus normalize time for both ionization stages by fixing the rising edge of the half-intensity point for the S XV resonance line (called $R$ henceforth) for both calculation and experiment. We then normalize the calculated intensity so that peak intensity of the $R$ for the calculated and observed peak are the same.

The data shown in Figs. 2(b) and 4(a) and 4(b) are the $R$ and S XVI Lyman-$\alpha$ line, Ly-$\alpha$, from a 2.1-$\mu$m-thick target with a sulfur-seeded dot of 300 $\mu$m in diameter. The target was irradiated with a 1-ns pulse focused to a 600-$\mu$m spot with $1.3\times10^{15}$ W/cm$^2$ of 0.53-$\mu$m light. In Fig. 2(b), the experimental $R$ and Ly-$\alpha$ line emissions are shown as a function of time in nanoseconds. Note that the time histories show an equal onset of the $R$ and Ly-$\alpha$, with a slow decaying Ly-$\alpha$ emission at late times. The line intensities in Fig. 2(b) have no experimental timing uncertainty beyond the $<50$-ps resolution of the streak spectrometer. Further, note that the foil burns through before the peak of the emission is observed and before the peak of the laser pulse.

In Figs. 4(a) and 4(b), the comparison of the calcula-

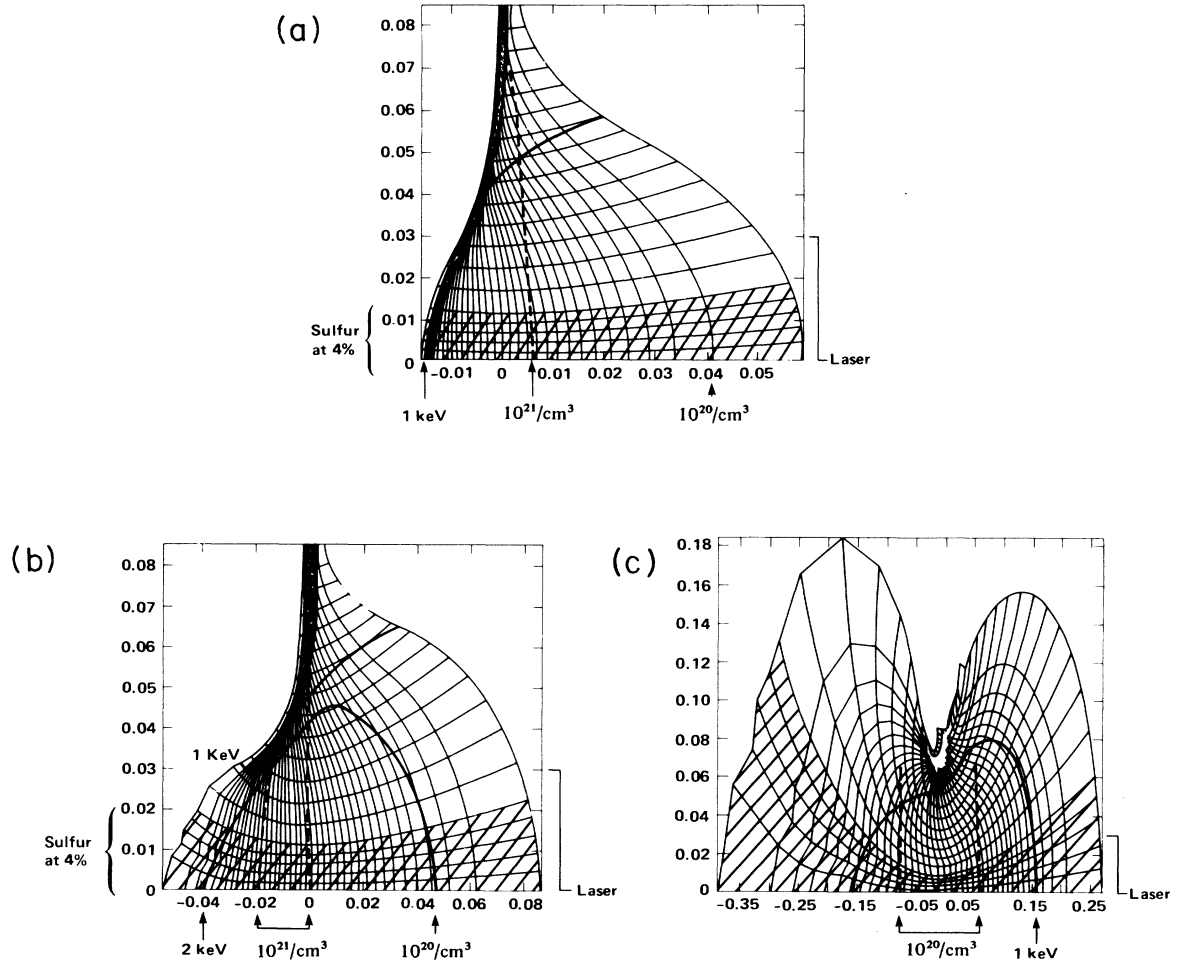


FIG. 3. Results of the two-dimensional simulation. Evolution of the foil is given for three times: (a) -0.6 ns, (b) -0.4 ns, and (c) + 0.6 ns. The peak of the laser pulse is at 0.0 ns and an intensity of $1.5\times10^{13}$ W/cm$^2$ of 0.53-$\mu$m light was used. The laser spot size of 600 $\mu$m, and a sulfur spot of 300 $\mu$m are shown.

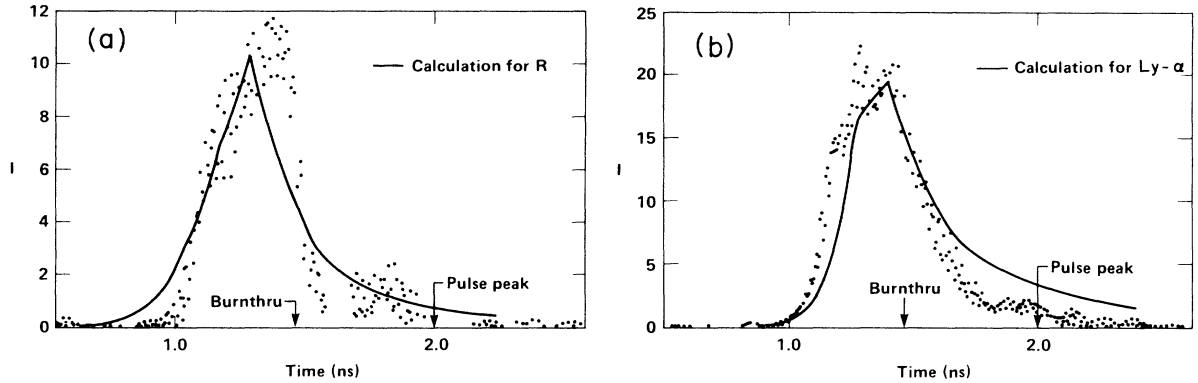


FIG. 4. Time-dependent emission for a 2.1-$\mu$m-thick foil with a 300-$\mu$m sulfur spot irradiated at $1.5\times10^{13}$ W/cm$^2$. The time is measured in ns; the peak of the pulse and burnthrough times are shown. (a) Comparison of calculation (solid curve) and experiment (dots) for the S XV $R$ emission. (b) Comparison of calculation (solid curve) and experiment (dots) for the S XVI Ly-$\alpha$ emission.

tions with the experimental data is shown for $R$ and Ly-$\alpha$, respectively. The overall agreement between the data and the calculation is quite good, i.e., the widths of time histories agree within 100 ps and the relative contribution of the S XV and S *XVI* emission are correct. However, the Ly-$\alpha$ time history shows a leading edge that starts more rapidly than calculated and decays more rapidly than predicted. This is a real discrepancy and not an artifact of the normalization scheme since the onset of the Ly-$\alpha$ and $R$ emissions are calculated to have a time delay of several 100 ps. This delay between the calculated Ly-$\alpha$ and $R$ cannot be attributed to temperature changes in the simulation, flux-limit changes, or rate coefficient changes. All of these possibilities have been tested as discussed below and the lag of Ly-$\alpha$ persists.

In Fig. 5 the ratio of the Ly-$\alpha/R$ emission versus time is shown for calculation and experiment. The experiment is represented as data points with the calculation shown as a solid line. Although the intensity time histories are individually in fair agreement, the ratios are in poor agreement at early time where there is large discrepancy with the onset times and in only adequate agreement at later times.

As a final comment on these data, the results for the S XVI and S XV principal quantum number 1-to-3 transitions show similar effects as the 1-to-2 transitions already discussed. The major difference is the weaker signal level in the 1-to-3 transitions.

For targets containing sulfur throughout the entire foil, the analysis requires inclusion of lateral gradients. Figure 6 shows the calculations for a 1-$\mu$m-thick $CH_x$ foil irradiated with a 1-ns-length pulse of 0.53-$\mu$m light focused to a 600-$\mu$m spot with an irradiance of $1.3\times10^{15}$ W/cm$^2$. The calculated time dependence of Ly-$\alpha$ emission is plotted versus time for various radial regions containing sulfur spots. For the curve labeled 150 $\mu$m the emission is integrated over the entire longitudinal direction (perpendicular to the foil) and integrated in the transverse direction over a spot of 150-$\mu$m diameter (75-$\mu$m radius) in the center of the laser spot. The curves labeled 300 and 900 $\mu$m represent integrations in the transverse direction over

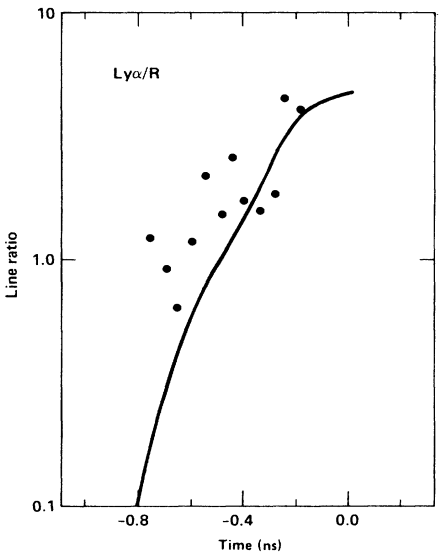


FIG. 5. Ratio of the intensity of the $R$ to Ly-$\alpha$ vs time, with zero time at the peak of the pulse. Experiment, solid curve; calculation, dots.

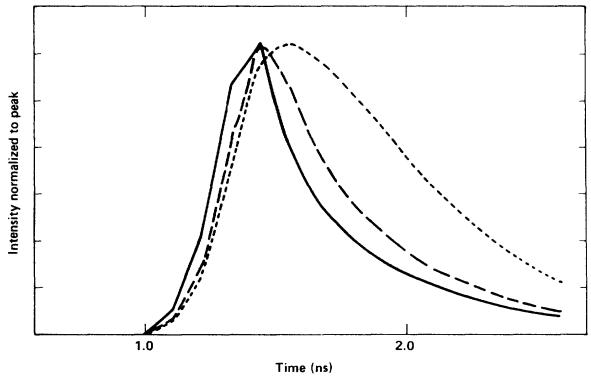


FIG. 6. Effects of integrating emission signal over various spot sizes. Integrated emission of $R$ vs time for three different spot sizes: 150 $\mu$m (——); 300 $\mu$m (— — —); and 900 $\mu$m (· · · ·). The conditions are same as those in Fig. 4.

a 300-$\mu$m spot and the entire target, respectively. For comparison purposes we have normalized the peak intensities equally for all cases. This figure shows that for the larger spots the emission rises slower on the leading edge. Also, the larger spots have a longer emission tail on the trailing edge of the pulse. This is because the sharp cutoff due to the burnthrough effect, which occurs before $t=2.0$ ns, is moderated by lateral transport of energy to the outer edges of the foil. This outer region of the foil will continue to emit sulfur lines since these regions have not become underdense. In Fig. 3, higher-density regions outside the laser spot can be seen which, at late times, reach temperatures capable of creating $K$-shell sulfur ions.

In Figs. 7(a) and 7(b), comparison of the data to the calculation for the uniform sulfur target is shown. In Fig. 7(a), the $R$ emission shows good agreement between calculation and experiment. Both the rising edge and the emission after burnthrough are in good agreement. It is only at late times that the long emission tail of the calculation is not reproduced. In Fig. 7(b) the Ly-$\alpha$ emission is shown to be poorly modeled. Here the thinner foil accentuates the underionization that is found in the calculations. Thus the lag in the Ly-$\alpha$ emission for the thicker 2.1-$\mu$m foil is translated into a long time emission as the lateral energy flow slowly ionizes the sulfur into and through the $K$ shell.

Note that even without a small seeded spot the modeling of these targets is still possible. Loss of information inherent in the data, which has integrated over both longitudinal and transverse gradients, in addition to having contribution from both directly illuminated and lateral energy transport heated areas, reduces accuracy of the diagnostic. Thus diagnosing the entire foil emission will provide only a small amount of information on the plasma parameters of this target.

Measurements have also been done at lower laser intensities to test the predictive capabilities. A $6\times10^{14}$ W/cm$^2$ laser pulse of 1 ns in a 900-$\mu$m focal spot has been focused on a 2-$\mu$m-thick $CH_x$ foil with 4% S uniformly added throughout the target. Due to the lower intensity, the plasma will be cooler and a different plasma temperature and density regime will be accessed.

In Figs. 8(a), 8(b), and 8(c), time histories of the emission of the $R$ and Ly-$\alpha$ are shown. In Fig. 8(a), experimental results for the two lines are compared. The $R$ emission in this case begins before the Ly-$\alpha$ emission by approximately 100 ps. The Ly-$\alpha$ is more intense at the peak with a rapid emission decay for both lines.

Figs. 8(b) and 8(c) the comparison of calculations with experiment are shown. The results of this comparison are favorable with the rise, peak, and fall of the emission well matched. Interestingly, in this case the ratio of the intensity of the $R$ to Ly-$\alpha$ is still poor even though the individual intensities compare well. The ratios would, if used as a diagnostic, indicate a higher ionization than the individual time histories. This would imply a higher temperature than predicted using the emission histories.

In summary, the present analysis succeeds in predicting many of the features of the data, but some discrepancies exist. The model, i.e., kinetics coupled to the hydrodynamics, predicts the general emission shapes qualitatively for all cases. The ionization balance at early times, represented by the S XV resonance line and the S XVI Ly-$\alpha$ line, is not well predicted. In fact the time delay predicted between the Ly-$\alpha$ and $R$ is not observed. The method also predicts the correct emission histories with the transverse gradients included. These results show that the experiments with emission from the entire surface can be modeled. However, the inherent loss of information, due to the widely varying plasma conditions contributing to the signal, diminishes the diagnostic value.

The present method sets bounds on the possible temperature ranges found with the hydrodynamics simulation. Since temperature diagnostics are difficult, the setting of limits is useful in the absence of a better alternative. The early time behavior is not due to errors in temperatures of the model. The simultaneous onset of the $R$ and Ly-$\alpha$ emission cannot be obtained by increasing the temperature within reasonable limits, i.e., a factor of 2 above the calculated temperatures. The early time emission, although not sensitive to the temperature as just mentioned, is dependent on the intensity of the laser. The

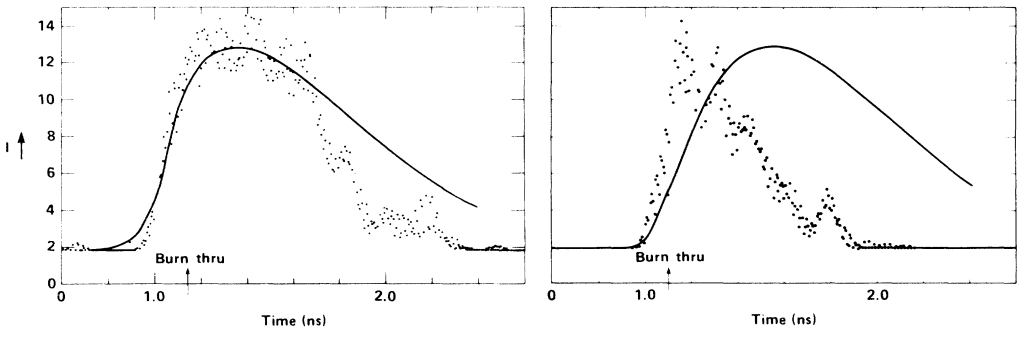


FIG. 7. Comparison of experiment to calculation for the emission as a function of time for a 1-$\mu$m-thick target with sulfur uniformly distributed, irradiated by a 1-ns, 0.53-$\mu$m laser pulse at $1.3\times10^{15}$ W/cm$^2$. (a) Comparison for $R$: Calculation, solid curve; experiment, dots. (b) Comparison for Ly-$\alpha$: Calculation, solid curve; experiment, dots.

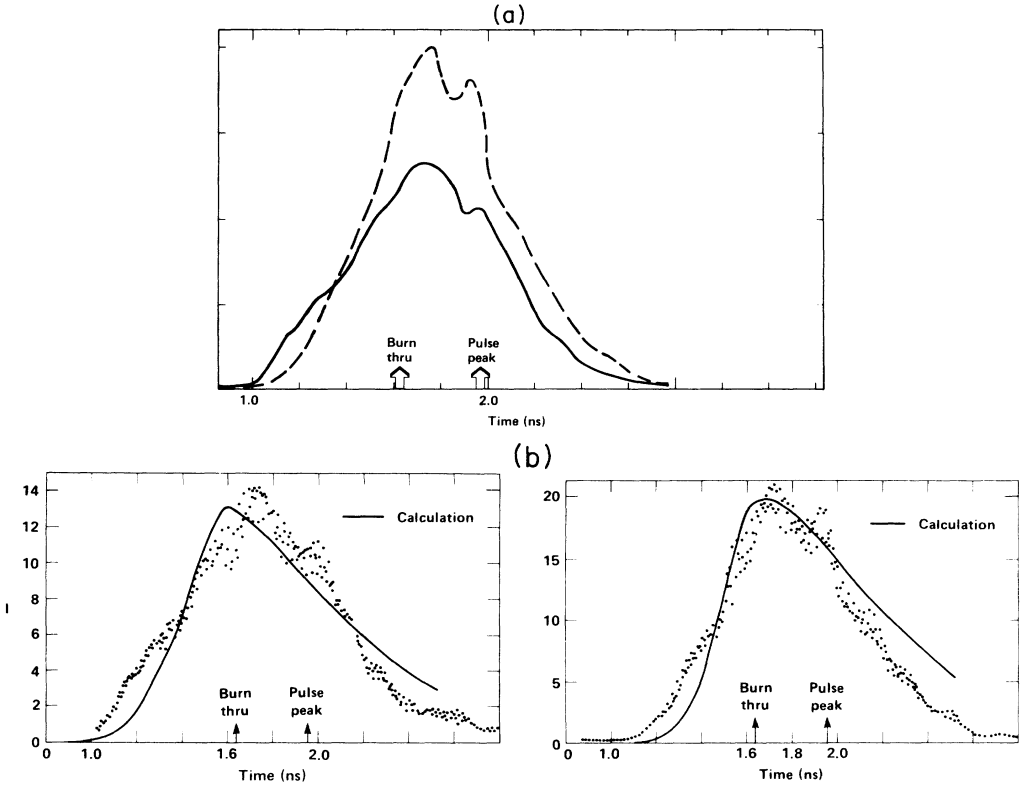


FIG. 8. Time-dependent emission from a 2.1-$\mu$m-thick foil seeded uniformly with sulfur irradiated at $6\times10^{14}$ W/cm$^2$ with a 1-ns, 0.53-$\mu$m laser pulse.

delay in the onset of the Ly-$\alpha$ emission is observed at lower intensity but not at higher intensity as observed by comparing Figs. 7 and 8. Finally, we note in all cases studied the emission decay at late times decreases more rapidly in the experiment than predicted.

## V. TESTING OF THE MODEL

To explain the ionization balance at early time we have tested the model by varying simulation parameters. Effects due to ionization rates have been tested in several ways. Increasing the rates in the kinetics code by a factor of 2 does not appreciably change the predicted emission histories. The lag in the Ly-$\alpha$ emission relative to the $R$ emission is due to the calculated rate of ionization. To obtain a simultaneous emission in the S XV and S XVI lines we would expect that the rate of ionization from S XV to S XVI and from S XVI to S XVII would have to be faster than the time resolution of the streak camera, i.e., $>50$ ps. This would indicate an ionization time of $2\times10^{10}$ sec$^{-1}$ while the calculated ionization time for a plasma with a temperature of 2 keV, and an electron density $10^{21}$ cm$^{-3}$ is $\sim3\times10^9$ sec$^{-1}$, which would yield a 150-ps time delay between S XV and S XVI. This assumes that the contribution from upward bound-bound collisions approximately doubles the ground-state ionization rate. To enhance the ionization rates by factors of 4 does not reduce the lag appropriately. Further, to test the effect of lower ionization stage rates on the calculated result, we initiated the simulation with all the population in the lithiumlike ground state. This resulted in a similar lag between the Ly-$\alpha$ and $R$ line emission. Finally, to test the possibility that simulation underestimates the temperature, we have multiplied all the temperatures by a factor of 2 and found that this still does not resolve the problem of the Ly-$\alpha$ and $R$ emission lag.

A second possibility is the electron flux limit used in the simulation to approximate the effects of nonlocal transport.[17] We have used a flux limit of 0.03 in the standard calculations, shown in the previous sections. This flux limit is optimum for matching the other observables in the experiment such as transmitted light and instability timing. When the flux limit is increased to 0.10, the plasma becomes hotter; however, the lag does not go away.

Third, there is the possibility of hot spots in the laser beam which increases local laser intensities. Modulation of the beam, in a pattern that varies the intensity by a factor of 2 or greater, is possible. However, the local temperature is a weak function of the laser intensity, i.e., $T\sim I^{2/3}$;[18] therefore, the intensity modulations would cause only slight temperature increases. In turn, the increased temperature, i.e., less than a factor of 2, would not be enough to explain the simultaneous emission of the $R$ and the Ly-$\alpha$, as discussed.

One possibility to explain the ionization balance, which we are currently not capable of calculating, is the effect of

nonlocal transport of energy. To obtain substantial ionization ~8-keV electrons are needed, i.e., electrons at approximately 3 times the threshold for ionization of S XV. The electrons must penetrate far enough ahead of the locally transported heat flux to produce substantial S XVI, so that no emission lag occurs when the heat front arrives. The difficulty is that for the conditions in our simulation we find that the ionization rate from these 8-keV electrons is about an order of magnitude lower than the dominant radiative recombination rate. Therefore, one can assume that there are not enough electrons at or above 8 keV in a Maxwellian distribution near the critical density surface to produce sufficient preionization.

The possibility does exist that the production rate of high energy electrons of energy $>8$ keV can be enhanced and then transported into the target. The production mechanism would most probably be resonance absorption since other high-energy electron production mechanisms require large regions of underdense plasma which would not have a chance to form in the early stages of the laser pulse.[19] The estimate of the electron density enhancement at 8 keV, relevant to the two laser intensities studies, are 6% and 4% due to the resonance absorption for the $1.3\times10^{15}$ and $5.9\times10^{14}$ W/cm$^2$, respectively. The hot electron temperatures which generate these fast electrons are 10 and 5 keV. The effective increase in the ionization rate of S XV, at a depth beyond the critical density surface, is calculated to be sufficient to sustain the ionization against the radiative recombination rate for the high-intensity experiment. However, in the lower intensity case the radiative rate dominates by more than an order of magnitude.

Thus a possible explanation of the discrepancy between the calculated and observed onset of the S XV and S XVI emission is the electrons produced by resonance absorption. The necessary ingredients, therefore, are the non-Maxwellian electron production together with nonlocal transport. The hydrodynamics simulation characterizes electron energy distribution as a one temperature, low-energy thermal group and an energy-resolved group at energies above the thermal. Although the nonthermal electron energies are resolved and transported, the kinetics simulation does not currently use the electron distribution but a temperature constructed of the mean total energy in the electron subsystem. Thus the kinetic model should have at least a two-temperature distribution to treat the effects in the ionization balance.

## VI. CONCLUSIONS

Present experiments coupled with simulations have illustrated a technique for diagnosing laser plasmas which effectively combines the strengths of both. The qualitative agreement is found to be good between the calculated time history of the emission of the S XV resonance line and S XVI Ly-$\alpha$ line, and the experimental observation. However, the quantitative agreement is still not correct. One area of difficulty is the late-time emission, i.e., after peak, which is calculated to be too intense for both S XV and S XVI transition. Second, the early time S XVI emission is calculated to lag the S XV for the high intensity experiments while the data show a simultaneous onset.

A number of important results can be derived from the experiment and analysis. First, the technique of keeping the concentration of the spectroscopically active element low has worked to overcome complications from radiative transfer, in particular, opacity variations, in the intensity of the diagnostic lines. This greatly simplifies the diagnostic procedure and decreases the uncertainty of the modeling. Second, use of the spot spectroscopy, for larger spot targets than were previously used, has been proven valid. Although the spots were 300 $\mu$m in diameter, we have shown with the simulation and observation that reduction of the transverse gradients can be achieved. This greatly simplifies the analysis and, as shown by comparison to data without spots, provides more information on the localized plasma. Third, detailed studies of the time histories of emission intensities are shown to be the correct quantities to study. The ratio of intensities are complicated, not only by a loss of information inherent in the ratio process, and leads to spurious diagnostics of the plasma. The usual case presented for the use of ratios in the relative contribution of the intensities would be more accurate than individual intensities. However, in the laser-produced plasmas, dynamics dominate the line emission and small discrepancies in predicting the time development of the emission can result, as shown in Sec. IV, in large discrepancies in the plasma conditions inferred from the intensity ratios. Fourth, even when the emission arises from a region which has gradients in only one direction, the simulation when performed in one dimension does not correctly represent the emission time histories. The two-dimensional simulation is therefore required.

Improved diagnostic techniques can also enhance the accuracy of the experiment. A space-resolved spectrometer with a time-resolved gated recording system could provide a snapshot of the entire spectrum to better correlate analysis using several lines. In addition, multiple frame interferometric probing of the electron density would provide an independent measure of the underdense plasma to confirm critical plasma parameters in the simulation. Use of other seed elements will allow probing of different parts of the electron distribution. If nonlocal heat transport and non-Maxwellian velocity distribution are the source of the discrepancies in the detailed comparison of the calculated and observed emission histories, other parts of the nonthermal distribution could be probed. In addition with improved resolution and spectral coverage, other spectral lines and other spectral techniques could be used. For example, the emission of the S XV $2\,^3P-1\,^1S$, and $2\,^1P-1\,^1S$, density, and the widths of the emission line profiles could yield electron density. Finally, as an essential, the experimental design should include an absolute timing fiducial for the time-resolving instruments.

The major calculational improvement which is dictated by the data analysis presented here would be the inclusion of actual electron distribution in the kinetic equations. Thus the calculated multigroup electron distribution could be coupled to cross sections to provide an improved kinetics model. This would overcome the difficulty found

in the present analysis where the high-energy electrons produced by resonance absorption are transported in the simulation, but a mean temperature is used in the kinetics model.

## ACKNOWLEDGMENTS

The authors gratefully acknowledge the work of Paul Drake for his work on the thin foil experiments and Steve Letts for the fabrication of the thin doped foil targets. The authors would like to acknowledge the Nova laser facility staff for operation of the facility and the Lawrence Livermore National Laboratory (LLNL) Laser Program for the support of this research. This work was performed under the auspices of the U. S. Department of Energy by the Lawrence Livermore National Laboratory under Contract No. W-7405-ENG-48.

[1]J. Nuckolls, L. Wood, A. Thiessen, and G. Zimmerman, Nature (London) **239**, (1972); J. J. Duderstodt and G. A. Mores, *Inertial Confinement Fusion* (Wiley, New York, 1982).

[2]M. H. Key, C. L. S. Lewis, J. G. Lunney, A. Moore, T. A. Hall, and R. G. Evans, Phys. Rev. Lett. **41**, 1467 (1978); B. Yaakobi, P. Burke, R. McCrory, W. Seka, J. M. Soures, A. J. Burke, and R. E. Deslattes, Opt. Commun. **38**, 196 (1981); D. L. Matthews, E. M. Campbell, N. M. Ceglio, G. Hermes, R. Kauffman, L. Koppel, R. Lee, K. Manes, V. Rupert, V. W. Slivinsky, R. Turner, and F. Ze, J. Appl. Phys. **54**, 4260 (1983).

[3]D. L. Matthews, P. L. Hagelstein, M. D. Rosen, M. J. Eckart, N. M. Ceglio, A. U. Hazi, H. Medecki, B. J. MacGowan, J. E. Trebes, B. L. Whitten, E. M. Campbell, C. W. Hatcher, A. M. Hawryluk, R. L. Kauffman, L. D. Pleasance, G. Rambach, J. H. Scofield, G. Stone, and T. A. Weaver, Phys. Rev. Lett. **54**, 110 (1985).

[4]R. L. Kauffman, R. W. Lee, D. L. Matthews, and J. D. Kilkenny, J. Quant. Spectrosc. Radiat. Transfer **32**, 335 (1984).

[5]P. G. Burkhalter, M. J. Herbst, D. Duston, J. Gardner, M. Emery, R. R. Whitlock, J. Grun, J. P. Apruzese, and J. Davis, Phys. Fluids **26**, 3650 (1983).

[6]M. H. Key, C. L. S. Lewis, J. G. Lunney, A. Moore, J. M. Ward, and R. K. Thareja, Phys. Rev. Lett. **44**, 1669 (1980).

[7]V. A. Bouko, S. A. Pikus, and A. Ya. Faenov, J. Phys. B **12**, 1889 (1979).

[8]M. Galanti and N. J. Peacock, J. Phys. B **8**, 2427 (1975).

[9]P. D. Carter, S. M. L. Sims, H. C. Barr, and R. G. Evans, Phys. Rev. Lett. **40**, 1177 (1978).

[10]D. W. Phillion, D. L. Banner, E. M. Campbell, R. E. Turner, and K. G. Estabrook, Phys. Fluids **25**, 1434 (1982).

[11]R. E. Turner, K. Estabrook, R. L. Kauffman, D. R. Bach, R. P. Drake, D. W. Phillion, B. F. Lasinski, E. M. Campbell, W. L. Kruer, and E. A. Williams, Phys. Rev. Lett. **54**, 189 (1985).

[12]D. T. Attwood, D. W. Sweeney, J. M. Auerbach, and P. H. Y. Lee, Phys. Rev. Lett. **40**, 184 (1978).

[13]Lawrence Livermore National Laboratory 1982 Laser Program Annual Report, 1983 (unpublished), Sec. II.

[14]R. L. Kauffman, T. Brown, and H. Medecki, Proc. Soc. Photo-Opt. Instrum. Eng. **427**, 84 (1983).

[15]G. B. Zimmerman and W. L. Kruer, Comments Plasma Phys. Controlled Fusion **2**, 51 (1975).

[16]R. W. Lee, B. L. Whitten, and R. E. Strout III, J. Quant. Spectrosc. Radiat. Transfer **32**, 91 (1985).

[17]A. R. Bell, R. G. Evans, and D. J. Nicholas, Phys. Rev. Lett. **46**, 243 (1981); J. P. Matte and J. Vermont, *ibid.* **49**, 1936 (1982); J. R. Albritton, *ibid.* **50**, 2078 (1983).

[18]C. E. Max, C. F. McKee, and W. C. Mead, Phys. Fluids **23**, 1620 (1980); Phys. Rev. Lett. **45**, 28 (1980).

[19]K. Estabrook and W. L. Kruer, Phys. Rev. Lett. **40**, 42 (1978).